RESEARCH ARTICLE

BATTERY ENERGY Open Access

WILEY

DBD plasma-assisted coating of metal alkoxides on sulfur powder for Li–S batteries

Ahmed Shafique[1,2,3] | Annick Vanhulsel[1,3] | Vijay S. Rangasamy[1,3] |
Kitty Baert[4] | Tom Hauffman[4] | Peter Adriaensens[2,5] |
Mohammadhosein Safari[2,3,5] | Marlies K. Van Bael[2,3,5] | An Hardy[2,3,5] |
Sébastien Sallard[1,3]

[1]VITO (Flemish Institute for Technological Research), Sustainable Materials, Mol, Belgium

[2]Institute for Materials Research (imo-imomec), Hasselt University, Hasselt, Belgium

[3]Energyville, Genk, Belgium

[4]Department of Materials and Chemistry, Research Group Electrochemical and Surface Engineering (SURF), Vrije Universiteit Brussel, Brussels, Belgium

[5]Imec vzw, division imomec, Diepenbeek, Belgium

Correspondence
An Hardy, Institute for Materials Research (imo-imomec), Hasselt University, Martelarenlaan 42, Hasselt B 3500, Belgium.
Email: an.hardy@uhasselt.be

Sébastien Sallard, VITO (Flemish Institute for Technological Research), Sustainable Materials, Mol 2400, Belgium.
Email: sallardsebastien@gmail.com

Abstract

Sulfur particles coated by activation of metal alkoxide precursors, aluminum–sulfur (Alu–S) and vanadium–sulfur (Van–S), were produced by dielectric barrier discharge (DBD) plasma technology under low temperature and ambient pressure conditions. We report a safe, solvent-free, low-cost, and low-energy consumption coating process that is compatible for sustainable technology up-scaling. NMR, XPS, SEM, and XRD characterization methods were used to determine the chemical characteristics and the superior behavior of Li–S cells using metal oxide-based coated sulfur materials. The chemical composition of the coatings is a mixture of the different elements present in the metal alkoxide precursor. The presence of alumina Al_2O_3 within the coating was confirmed. Multi-C rate and long-term galvanostatic cycling at rate C/10 showed that the rate capability losses and capacity fade could be highly mitigated for the Li–S cells containing the coated sulfur materials in comparison to the references uncoated (raw) sulfur. Electrochemical impedance spectroscopy (EIS) and cyclic voltammetry (CV) confirm the lower charge-transfer resistance and potential hysteresis in the electrodes containing the coated sulfur particles. Our results show that the electrochemical performance of the Li–S cells based on the different coating materials can be ranked as Alu-S > Van-S > Raw sulfur.

KEYWORDS
electrochemistry, lithium, material science, sulfur

1 | INTRODUCTION

Over the last few decades, technological progress towards a more environmentally friendly and energy-saving society has been gaining momentum across the world. Therefore, one of the foremost technological challenges of this century is to increase the production and storage of renewable energy. Many countries have already decided to eliminate, in the very near future, the use of fossil fuels (due to global warming) and combustion engines with wind and green electric vehicles in the transport sectors.[1,2] To fully utilize the electricity generated by these alternative energy sources, rechargeable battery systems play a vital role.

Among all the rechargeable battery systems, use of lithium-ion (Li-ion) batteries is currently considered to be the most attractive solution due to their low self-discharge rate, high cell voltage, and stable cycling performance.[3,4] However, the use of insertion materials (such as $LiMn_2O_4$, $LiNiMnCoO_2$ $LiFePO_4$, and $LiCoO_2$) for positive electrodes is limited to a specific capacity of <170 mAh/g, which limits their energy density drastically. Furthermore, the standard positive electrode materials are becoming increasingly more scarce (e.g., nickel and cobalt) and are further limited by their high cost, high weight, and safety concerns, which restrict their further use in more sustainable large-scale power systems. Therefore, to fulfill the criteria of requirement of high energy density and low cost for modern technology, more sustainable and low-cost, lightweight materials must be explored.[2–5]

Among different potential candidates, sulfur seems promising as a positive electrode material, with five times higher theoretical capacity (1675 mAh/g) and energy density (2500 Wh/kg) than standard positive materials for Li-ion batteries.[6,7] Besides, sulfur is a very abundant, low-cost, nontoxic, and lightweight element with a low environmental footprint, which makes the Li–S battery more sustainable and less dependent on critical raw materials for manufacture. Despite these advantages, there remain many challenges to practical applications of Li-S batteries. It is known that sulfur typically undergoes large volume expansion (~80%, when reduced to Li_2S) during the battery discharge, has poor electronic conductivity (~5 × 10^{-30} S/cm), and dissolution of intermediate polysulfides into the electrolyte takes place (i.e., the polysulfide shuttle effect).[8,9] These issues eventually lead to loss/low utilization of the active material, low Coulombic efficiency, limited charge rate, and rapid capacity decay at the cell level and hinder the commercialization of the Li–S battery system.[10] In recent years, to alleviate these problems and to improve the performance of Li-S batteries, considerable efforts have been made, including the use of modified separators or lithium anodes, optimization of the liquid electrolyte composition (using electrolyte additives), optimization of the binder composition, or use of an appropriate sulfur/electrolyte ratio.[11–14]

In addition, R&D efforts have been focusing on the development of sulfur positive electrodes.[12,15,16] Various strategies have been developed to combine sulfur with conductive matrices by using layered porous carbon, graphene sheets, and carbon nanofibers/nanotubes.[17–20] These strategies are normally adopted because conductive matrixes can simultaneously serve as a physical barrier to hinder the lithium polysulfide shuttle phenomenon and to improve the utilization of sulfur (limited sulfur bulk, high surface contact with a conductive matrix). However, these physical routes are not able to solve all problems concerning Li–S batteries.[21–23] Due to the weak interaction between the nonpolar carbon host and polar polysulfides, large capacity fading has been observed during long-term cycling. Consequently, the polysulfides leak out of the composite and the physical trapping becomes ineffective with prolonged use of Li-S batteries. In another strategy, different metal oxide and conductive polymer additives are used to trap the dissolved intermediate polysulfides in the positive electrode.[22–25] It is reported that these additives function as a polysulfide reservoir and effectively improve the rate performance and cycling stability of Li–S batteries. However, using the synthesis procedures (using thermo-treatment and ball milling), it is difficult to ensure homogeneous dispersion of carbon with sulfur, resulting in low sulfur utilization and limited battery performance.[21,26,27]

Compared with the above-mentioned strategies, the surface coating strategy is considered to be effective in preventing the dissolution of lithium polysulfides and in improving the electrochemical performance of the Li–S battery system.[9,12,15] Recently, surface coating of sulfur particles using inorganic metal oxide compounds (such as MgO, Al_2O_3, V_2O_5, SiO_2, CaO, MoO_2, TiO_2, ZrO_2, etc) has been explored with much interest.[23,28–30] The interest in these intrinsically polar metal oxides is mainly due to three key functions[28,30]: (i) Compared to carbon materials, metal oxides provide abundant polar active sites for adsorption of polysulfides. Metal oxides that usually contain an anion of oxygen in the oxidation state of (O^{2-}) always have a strong polar surface. Besides, due to the strong bonding between the metal and the oxygen, metal oxides tend to be insoluble in most organic solvents. However, although in the literature[23,28,29] it has been reported that metal oxides have the ability to capture polysulfides, the detailed adsorption mechanism is still not clear. (ii) Some nonconductive oxides act as

transporters of polysulfides, i.e., the metal oxide material transports the polysulfides (Li_2S_x) from the poorly conductive oxide surface to the highly conductive carbon matrix. The latter will further ensure full electrochemical conversion. (iii) The use of metal oxides limits the inhomogeneous reactions of the sulfur species, especially the precipitation step (Li_2S_4 and Li_2S in discharge, S_8 in charge), and thus mitigates the capacity fading.

The reported processes for surface coating of sulfur powder (using different metal oxides) are mostly hydro-thermal or wet chemical processes (i.e., sol–gel) that require additional solvent and energy-intensive drying steps, which renders the process insufficient for most practical and sustainable upscaling applications. Besides, the upscaling of other reported deposition techniques on powders like atomic layer deposition (which requires more time for chemical reactions and is an energy-consuming sensitive process) or chemical vapor deposition (which requires temperatures above 500°C, which are not suitable for sulfur) is also rather limited.[12,31–36] More importantly, the sublimation of sulfur must be considered during the heat treatment or low-pressure steps. Hence, the development of simple techniques to prepare coated sulfur without heat treatment, at ambient pressure, and with limited processing time is of interest technologically and in terms of cost.[10,16,37,38] To the best of our knowledge, no reports have been published on metal oxide-coated sulfur particles for Li–S batteries that fulfill these requirements.

In our previous publications,[39,40] we reported an alternative approach for coating commercial sulfur powder with a conductive polymer film using atmo-spheric dielectric barrier discharge (DBD) plasma tech-nology. The benefits of this process are the low temperature, no solvent, ambient pressure, low energy consumption, and compatibility for sustainable technol-ogy up-scaling. The conductive coating resulted in increased particle conductivity, resulting in an improve-ment of the electrochemical properties (i.e., higher capacity, lower capacity fading, and improved kinetics). In the current work, we have extended the coating of sulfur particles by the DBD-plasma coating process using different metal alkoxides as coating precursors. In the literature,[26,41,42] compared to non-modified sulfur pow-der, alumina-based coating on sulfur is widely reported and considered to be the state of the art, especially considering its polysulfide trapping capability and excellent Li–S cell performance (it is more stable, has higher specific capacity, and improved rate capability). Besides, vanadium-based coating (crystalline) is reported to be the most efficient polysulfide trapper, which also acts as an electrocatalyst.[22,43] To the best of our knowledge, no direct coating of sulfur particles by

DBD-plasma using these metal oxide-based materials has been reported in the literature. This work focuses on the atmospheric plasma deposition of aluminum-and vanadium-based coatings on sulfur particles, characteri-zation of the coated sulfur materials, and investigation of the electrochemical performance of these modified sulfur materials.

2 | EXPERIMENTAL SECTION

The sulfur powder (purchased from Merck, 99.0%–101%) was sieved at 50 μm before use. An atmospheric DBD-plasma process was developed that enabled a metal oxide-based coating of sulfur particles. For more details on the process, experimental conditions, and evolution of key parameters, please refer to our previous publica-tion.[39] Aluminum sec-butoxide (Alfa Aesar, >97%) and vanadium (V) oxytriethoxide (Sigma-Aldrich, >95%) were used as coating precursors. The plasma treatments were performed at a frequency of 18 kHz and 500 W plasma power. The Ar gas flow was fixed at 30 slm with the addition of 1.5 slm O_2, and the total processing time was set at 25 min. The precursor injection dose for each precursor was set to 75 mg/min. In this way, the Alu–S and Van–S samples were obtained using the alumina and vanadium oxide precursors, respectively. In addition, for optimum precursor dosing in the case of aluminum sec-butoxide, it is necessary to preheat (50°C) the precursor to reduce its viscosity and enhance the precursor atomization during the plasma process.

To study the structural phases in the deposited coatings, X-ray diffraction (XRD, Empyrean) patterns were recorded using monochromatic Co–K$_\alpha$ radiation at 40 mA and 45 kV, with diffraction patterns recorded at a scan speed of 0.067335°/sec between 10° and 90°. The particle size distribution (PSD) of the sulfur powders was measured using a Microtrac S3500 particle size analyzer. The particle morphology of coated and uncoated sulfur powders was characterized by scanning electron micro-scope (SEM) using an EDS detector from FEI™ Nova NanoSEM 450 using secondary electron images taken using a CBS detector and an acceleration voltage of 5 kV, with all the measurements being performed in a vacuum chamber. Coated powders were investigated by XPS measurements using a PHI-5600ci spectrometer (Al source + monochromator/Survey + Multiplex (high reso-lution) 0.1 eV/step–pass energy: 23.5 eV-measured area: Ø 800 μm). The powders were applied on an Indium foil (pressed into this soft metal). For a number of samples, the neutralizer was used to reduce the "charging" problem at the samples during the measurements (the nonconductive nature of the sample led to a large shift

and broadening of the peaks in the spectra). Solid-state ^{27}Al-MAS NMR spectra were acquired on an Agilent VnmrS Direct-Drive 400 MHz spectrometer (9.4 Tesla) equipped with a T3HX 3.2 mm probe. Magic angle spinning was performed at 14 kHz. The signal of $AlCl_3$ was used to calibrate the aluminum chemical shift scale (0 ppm). The acquisition parameters used were as follows: a spectral width of 420 kHz, a 90° pulse length of 4 μs, an acquisition time of 10 ms, a recycle delay time of 5 s, and about 65,000 accumulations.

The impact of the developed coatings on battery performance was studied in coin cell cycling tests. The coated and uncoated sulfur-based electrodes were prepared using an established protocol.[14,39] A tape casting method was followed to obtain sulfur-based positive electrodes by mixing sulfur (66 wt.%): carbon-black C-nergy Super-C65 (24 wt.%): LiPAA- binder (10 wt.%) using mechanical stirring at 650 rpm for 15 min. The carbon black powder C-nergy Super-C65 (Imerys Graphite & Carbon) was sieved at 150 μm. A LiPAA (lithium polyacrylic acid, a polyelectrolyte) binder aqueous solution was prepared as reported previously.[14] The slurries were coated using the doctor-blading technique on a carbon-coated aluminum foil (MTI-KJ group) and dried in a fume-hood at room temperature. The electrodes were punched, weighed, and dried overnight in a desiccator and then briefly under vacuum for 15 min before being used. To ensure a fair comparison, the average sulfur loading was calculated to be ~4.5 mg/cm^2 for all composite sulfur electrodes (15 mm diameter, geometrical surface area ca. 1.77 cm^2). Electrochemical measurements were conducted in CR2032 coin cells. The cells were assembled in an argon-filled glovebox (Jacomex GP-concept) with lithium metal (16 mm diameter, 750 μm thickness) as the negative electrode, a polymeric separator (Celgard 2400, 19 mm diameter), and an electrolytic solution (90 μL, SoulBrain MI) of lithium bis(trifluoromethanesulfonyl)imide (LiTFSI) 1M in dimethoxyethane (DME):1,3-dioxolane (DOL) with 2:1 as the weight ratio. LiNO₃ (Aldrich, 99.99° trace metal

basis) was added to reach a 5% weight ratio. The coin cells were equilibrated for 6 h at OCV and then cycled over a voltage range of 1.5–3.0 V versus Li$^+$/Li. Galvanostatic (dis)charge tests were carried out using a BioLogic battery testing system. The cells were tested using different protocols, either at a single C-rate (C/10) for a long cycling test or different charge/discharge rates with C/10 for the first 30 cycles, followed by C/5, C/2, 1C, and C/10 rates with 10 cycles for each step. Cyclic voltammetry (CV) tests were performed from 1.0 to 3.0 V versus Li$^+$/Li at a scan rate of 0.1 mV/s. The scan rate of the linear sweep voltammetry (LSV) tests was 0.1 mV/s over a voltage range of 1.5–5.0 V versus Li$^+$/Li. In the electrochemical impedance spectroscopy tests (using Ametek PARSTAT PMC-1000), cells were left at OCV for 1 h before characterization in the frequency ranges between 10 mHz and 300 kHz.

3 | RESULTS AND DISCUSSION

3.1 | Material characterization

A color difference is observed between the uncoated and plasma-coated sulfur powders (Figure 1). The commercial raw sulfur is yellow, whereas Alu-S and Van–S-coated sulfur powders are greenish-yellow. This color difference is attributed to the coating material on the sulfur powder. The cumulative PSD (particle size distribution) is very similar (if not identical) for all coated and uncoated samples (Supporting Information: Figure S1). As expected, before the coating step, the positive effect of the sieving (below 50 μm) is evident from the narrowing of the PSD of the raw sulfur powder. We observe a small increase in the average particle size of the Alu-S- and Van–S-coated sulfur powders when compared to the raw sulfur. This is attributed to slight aggregation during the formation of the coating. We suppose that during the coating initiation and growth, it can act like an adhesive for neighboring sulfur particles.
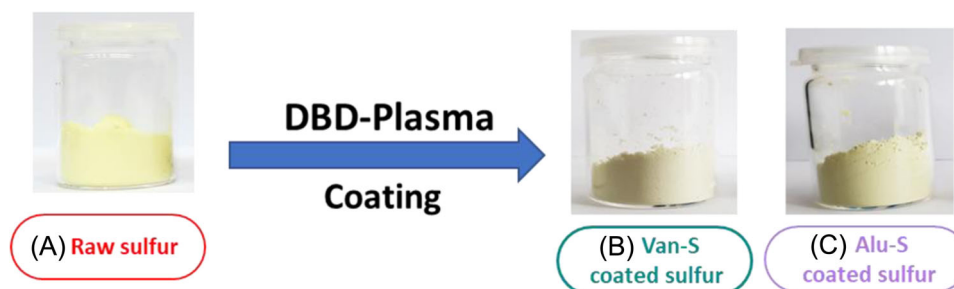

FIGURE 1 Selection of (A) raw (uncoated) and (B) Van–S-coated and (C) Alu–S-coated sulfur powders. Alu–S, aluminum–sulfur; Van–S, vanadium–sulfur.

—WILEY—

The loss of the finest powder fractions during processing is very unlikely as no significant difference is observed for the PSD of the raw, Van–S, and Alu–S powders for particles with a diameter of 10 μm and lower. Measurements of the electrical conductivity using our in-house apparatus[39,40] did not allow us to measure significant changes between the raw sulfur and the Van–S and Alu–S powders. Then, the electrical conductivity of the coated sulfur powders was found to be lower than
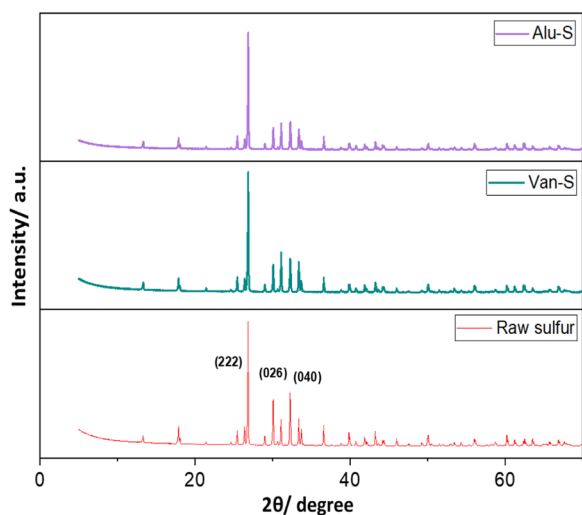
10^{-12} S/cm. It appears reasonable to consider the coating to be nonconductive and this is confirmed by the XPS analysis (see discussion later).

X-ray diffraction (XRD) analysis (Figure 2) provides details about the crystal structure of the coated and uncoated sulfur powders. The standard sulfur crystal structure patterns are observed, showing various sharp peaks between 15° and 70°. All the diffraction peaks in the pattern of (Alu–S and Van–S) coated and raw sulfur powders show two prominent (222) and (040) reflections at around 26° and 32°, also smaller peaks, which fit ICDD (no. 01-078-1889) without any impurity phase.[21,26,44,45] This corresponds to standard and similar patterns of sulfur with an Fddz–orthorhombic structure. The sulfur powders with different coatings present the same diffraction pattern compared to raw sulfur. This indicates that the coatings are amorphous and/or too thin to be measurable in XRD.

SEM analysis (Figure 3 and Supporting Information: Figure S2) was carried out to study the morphology of the coated and raw sulfur particles. In comparison with raw sulfur and irrespective of the different types of precursors used, all coated samples show the same morphology and particle size. This observation is consistent with the PSD results (Supporting Information: Figure S1). In addition, the surface of the (Alu–S and Van–S) coated sulfur particles is clearly changed in comparison to the raw sulfur (Figure 3C and Supporting Information: Figure S2A). Any significant etching of the sulfur surface
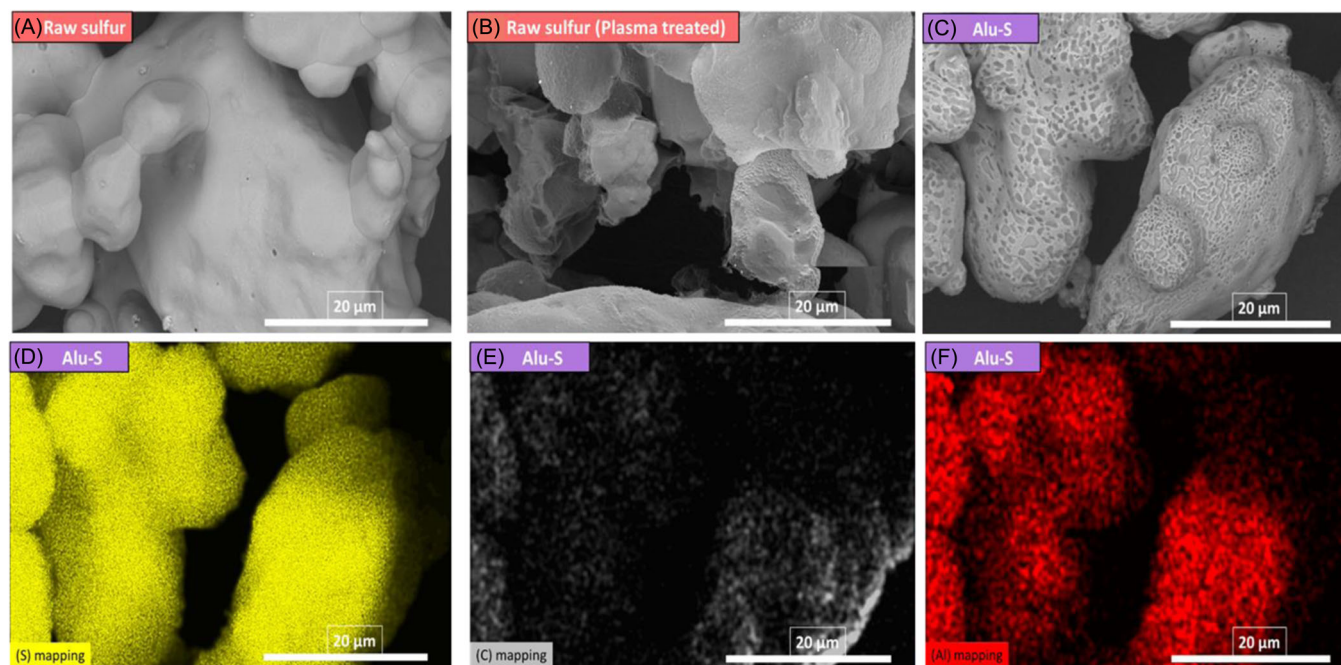

FIGURE 2 XRD patterns of raw sulfur and (Alu–S and Van–S) coated sulfur samples. Alu–S, aluminum–sulfur; Van–S, vanadium–sulfur.

FIGURE 3 SEM images of (A) raw sulfur, (B) raw sulfur plasma-treated, (C) Alu–S-coated sulfur, and (D–F) corresponding EDS mapping analysis revealing the presence of elements sulfur (S), carbon (C), and aluminum (Al). Alu–S, aluminum–sulfur.

by pitting induced by the plasma process is considered to be negligible. This is confirmed by exposing the raw sulfur to the same plasma field (without any coating precursor present). In that case, we did not observe any significant surface change (Figure 3B). The EDS imaging on Alu–S and Van–S-coated samples (Figure 3C–F, and Supporting Information: Figure S2) confirms the deposition of the different metallic elements (Al and V) on the surface of the sulfur particles. In addition, the metallic elements appear to be homogeneously distributed over the surface of the sulfur particle. The EDS elemental mapping indicates that the spatial distributions of the aluminum and vanadium elements (Figure 3F and Supporting Information: Figure S2D) on one side and the sulfur element on another side (Figure 3D and Supporting Information: Figure S2B) are at least very similar. The change in the local concentration (color intensity) is attributed to the geometrical effect of the nonflat surface of the sulfur particles. Consequently, it appears reasonable to consider that the metallic elements are homogeneously present on the surface of the sulfur particles at least at the submicroscopic scale. Note that for the Alu–S and Van–S materials, carbon seems to be significantly present on the surface of the coated sulfur particles. However, SEM/EDS analysis does not allow differentiation of the ubiquitous carbon contamination and carbon present in the DBD plasma coating.[39]

XPS analysis (Figure 4, Supporting Information: Figures S3 and S4) was carried out to characterize the chemical composition of the surface of the different sulfur powders. The elemental surface composition is considered significantly different (as expected) for the raw and the coated sulfur samples (Table 1). The carbon detected on the surface of the raw sulfur is attributed to atmospheric adventitious contamination. The carbon surface content increases from ~9% for the raw sulfur

samples to ~30% for the coated sulfur samples. This indicates the hybrid (organic/inorganic) nature of the plasma-polymerized coatings in which organic fractions from the alkoxide group are incorporated during coating deposition.[39] Consequently, we consider that the C1s spectra of the coated and uncoated sulfur powders show (Supporting Information: Figure S4) the main peaks measured at 285.1 eV, which can be attributed to the hydrocarbon carbon species of C–C (sp^3) groups. This is consistent when considering the source of the carbon atoms present in the coating to be mainly the alkoxide groups of the metallic precursors. Therefore, we consider these coatings not to be conductive, in agreement with our electrical conductivity measurements. In addition, the XPS analysis survey spectrum (Supporting Information: Figure S3) is collected on Alu–S-coated sulfur samples with the main peaks indexed to rule out the presence of any impurities or the presence of components beyond the expected composition. As described in the XPS analysis in our previous article,[39] sulfur is still detected on the surface of the coated powders, even at a low percentage of ~16–18. This can either be explained by the coating thickness being thinner than the XPS sampling depth and/or the fact that the coatings show pin holes that are not visible on the SEM images. This means that a proportion of the surface of the sulfur particles can remain uncovered (i.e., discontinuity in coverage by the aluminum precursor), even if this effect cannot be clearly identified in the SEM images (Figure 3 and Supporting Information: Figure S2).

Taking into account that the range of the escape depth of photoelectrons for a standard XPS apparatus is several nanometers (~10 nm maximum), we consider that the coatings formed by the DBD-plasma treatment have thicknesses that are (typically) in the range of several nanometers, and this is in agreement with the low intensity of the signals (Figure 4 and Supporting
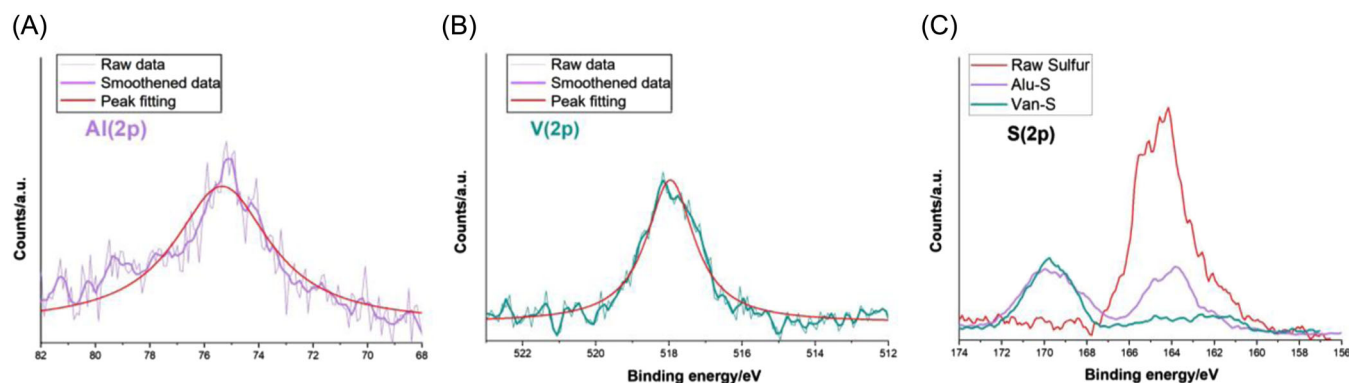

FIGURE 4 XPS (A) HR Al2p-spectra of Alu–S-coated sulfur, (B) V2p-spectra of Van–S, and (C) S2p spectra of raw and (Alu–S and Van–S) coated sulfur. Peak fitting is adjusted and peaks are smoothed by 5pts Savitzky Golay. Alu–S, aluminum–sulfur; Van–S, vanadium–sulfur.

TABLE 1 Elemental surface composition (XPS) of coated and uncoated samples (atomic percentages).

Sample	Carbon (%)	Oxygen (%)	Nitrogen (%)	Sulfur (%)	Aluminum (%)	Vanadium (%)
Raw Sulfur	9	—	—	91	—	—
Alu–S	33	39	9	18	1	—
Van–S	28	48	7	16	—	<1

Information: Figure S4). The presence of the aluminum and vanadium elements on the surface of the coated Alu–S and Van–S materials is confirmed from the Al2p and V2p spectra (Figure 4), in agreement with the EDX mapping (Figure 3 and Supporting Information: Figure S2). The amount of metal elements may appear very limited, but different parameters must be considered. First, the coating is very thin; thus, the sensitivity of the XPS equipment itself is pushed to its limit. Second, other elements present on the surface could influence the signal/noise ratio for the Al and V elements. The plasma process, using metal alkoxides $Al[OCH(CH_3)C2H_5]_3$ and $VO(OC_2H_5)_3$ as the precursors, cannot lead to the formation of a pure metal oxide coating. The elements of alkoxides, carbon, and oxygen cannot be removed during the plasma processing and are incorporated into the coating. The ubiquitous contamination of the sample during transport cannot be avoided. From the Al2p spectrum (Figure 4A), the peak at 74.9 eV is assigned to the Al^{3+} oxidation, which is in agreement with the presence of Al_2O_3 (amorphous). One can consider that the energy resolution of our survey scan is too poor to reach such a conclusion but it also corresponds to the oxidation state of the alkoxide precursor and is consistent with the NMR analysis data (see Figure 5 and related discussion).[41,45,46] Similarly, for the V2p spectrum (Figure 4B), the peak at 517.5 eV is assigned to the V^{5+} oxidation. First, we could potentially claim that the V^{5+} is compatible with the presence of V_2O_5 (amorphous), but the latter is not detected by solid-state NMR analysis, contrary to Al_2O_3 (see related discussion on NMR below). Second, the presence of a residual vanadium precursor that has not fully reacted during the coating process must also be taken into account.[47–49]

The presence of nitrogen and oxygen observed in coated samples (Table 1) is ascribed to the incorporation of nitrogen and/or oxygen during the plasma process and/or postcontamination of the coating when exposed to air. Figure 4C shows the S2p spectra for the raw and (Alu–S and Van–S) coated sulfur. The peaks at 164.0 and 165.2 eV can be assigned to the $S2p_{1/2}$ and $S2p_{3/2}$ spin–orbit levels of sulfur.[45] The sulfur spectra confirm that the S–O bonds were formed upon plasma treatment by the presence of the peak at 169.6 eV for the plasma-treated sample.[39,40]
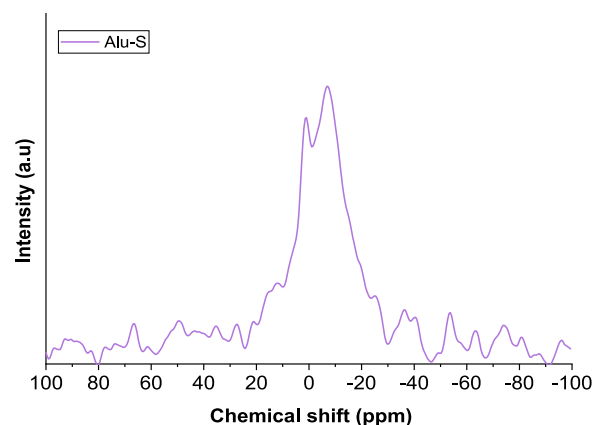

FIGURE 5 ^{27}Al solid-state NMR spectrum of Alu–S-coated sulfur powder, signals attributed to Al_2O_3. Alu–S, aluminum–sulfur.

Consequently, the sulfur particle surface is significantly (i.e., S–O) oxidized. The oxygen element can be present either as adsorbed oxygen (contamination), incorporated within the carbon, or in the metallic domains of the coating. It appears that the XPS data do not show a significant difference between the Van–S and Alu–S samples, except for the respective presence of the vanadium and aluminum elements.

In Figure 5, the solid-state ^{27}Al-NMR spectrum of the Alu–S-coated sulfur powder confirms the presence of an alumina-based coating for the sulfur sample, that is, Al_2O_3 metal oxide is undoubtedly detected. NMR analysis of the alumina-based coating is very challenging and the literature is very limited concerning the effect of plasma-deposited coatings, making a full identification of the coating difficult. The signals of alumina can be observed in the spectrum at chemical shift positions (in ppm) expected from the literature.[50–52] However, the signals are weak, confirming that the coating is relatively thin (nanocoating). In addition, it is also possible that only some of the aluminum atoms of the coating are incorporated within the alumina. The main peaks between −10 and 5 ppm are attributed to octahedral alumina and are in agreement with the simulated results reported in the literature.[50–52] However, the signals attributed to alumina are broader, which indicates a lower degree of chain length. This reveals

that, as expected, the plasma-polymerized metal oxide-based coating presents certain inhomogeneities at the micrometric scale compared to coatings obtained using standard chemical/electrochemical methods.[50,53,54] In addition, certain sub-products and groups may potentially be formed and can either remain as it is or incorporated into the main alumina alkoxide chain created by DBD-plasma. These results are also in agreement with XPS spectroscopy data reported previously in Figure 4. On the other hand, no ^{51}V-NMR signal could be detected for the Van–S sample. This suggests that a significant difference exists in the coating present on the Alu–S powder sample in comparison to the Van–S powder either in terms of the coating macrostructure (thickness, coverage) or the coating microstructure (chain level), which could relate to the fact that the performance of the Van–S-based Li–S cell is less pronounced in comparison with Alu–S cells (see Section 3.3 and related discussion).

To summarize, the coated sulfur materials created by the DBD-plasma deposition of alkoxide precursors present a thin coating (nanometric thickness) on sulfur particles. The coverage and thickness of the coatings are homogeneous at least at the submicrometric scale. Each coating, in addition to the desired metal oxide, contains a significant amount of carbon due to the plasma polymerization process. In the DBD process (reactor), when the alkoxides are activated, the remaining organic parts can be trapped in the growing coatings. The coatings are considered to be nonconductive. The oxidation state of the metallic element present in the coating is similar to the one of the precursor used. The presence of metal oxide Al_2O_3 could be confirmed for the Alu–S materials, while vanadium oxide could not be convincingly detected on the Van–S-coated samples. Sulfur atoms on the surface of the particles are significantly oxidized (which suggests that the coating is not fully homogeneous) due to the DBD-plasma process itself and it is difficult to estimate how the oxidized sulfur atoms can influence the electrochemical properties of the coated sulfur materials.

3.2 | Pristine electrode (SEM) characterization

The electrodes prepared with raw sulfur-, Alu–S-coated, and Van–S-coated powders were investigated by SEM to determine the effect of coated sulfur powders on the morphology of the positive electrodes. Figure 6 shows the top surface of the electrodes in a pristine state (before cycling). The pictures show that the morphology of all uncoated and coated sulfur electrodes is generally identical at a micrometric scale. These results are

comparable with those described in our previous work,[14,39] where we reported that the morphology and porosity of both coated and raw sulfur electrodes (using the water-based protocol and LiPAA as a binder) are similar in pristine and cycled states. Based on these results, as expected, we rule out any influence of an (Alu–S and Van–S) coating layer on the morphological stability of the electrode, which means that the porosity and structural integrity of the electrode are maintained intact.

3.3 | Electrochemical characterization

Figure 7A–D represents the cycle number versus specific discharge capacity evolution at C/10 of the Li-S cells with both pristine and (Alu–S and Van–S) coated sulfur-based positive electrodes. To check the repeatability of the cells, five Li-S cells from each sample were prepared, assembled, and tested by the same operator. As anticipated, in comparison with raw sulfur, the reproducibility is improved for Li–S cells containing the (Alu–S and Van–S) coated sulfur powder. This clearly shows that the different coated sulfur materials show good homogeneity and better electrochemistry for both pristine and aged positive electrodes. We compared the data of Li–S cells (Figure 7D) considered as "most representative," that is, the Li–S cells showing the most regular evolution of the specific capacity versus aging. For the reference raw sulfur Li–S cell, the initial specific capacity is ~820 mAh/g. Besides, all (Alu–S and Van–S) coated sulfur samples present inferior (~350–600 mAh/g) initial specific capacity. This effect can be ascribed to the activation of the coating on sulfur particles (see later and related discussion). However, after a few cycles, all cells present specific capacities between 500 and 700 mAh/g. For most of the Li–S cells, especially the cells containing the raw sulfur, the discharge capacity decreased rapidly with aging. A reasonable explanation for the rapid aging of Li–S cells is the high mobility of the long-chain polysulfides in the DOL/DME-based electrolyte, which leads to the well-known redox-shuttle phenomenon. The long-chain polysulfides can diffuse away from the cathode and reach the lithium anode, where they enter the passivation films on the lithium electrode. This irreversible loss of polysulfides translates into the loss of the sulfur reservoir of the cell and results in capacity loss during the subsequent cycles. This capacity loss is pronounced during the initial cycles and gradually levels off to a lower rate of aging thanks to the passivation of the lithium electrode, among other parameters, depending on the parameters of the cell design. For instance, the gradual saturation of the electrolyte by the polysulfides
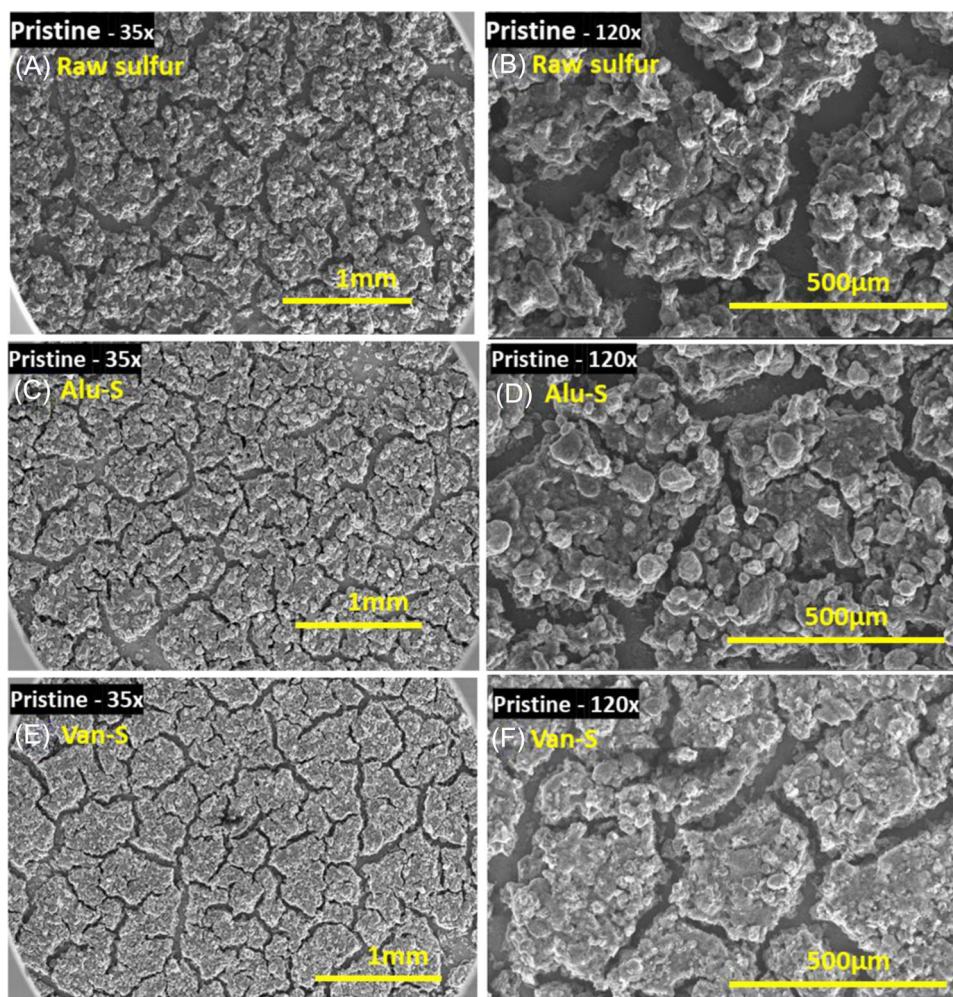
FIGURE 6 SEM images of sulfur electrodes in a pristine state with raw (A,B), Alu–S-coated (C,D), and Van–S-coated (E,F) sulfur powders at different magnifications. Alu–S, aluminum–sulfur; Van–S, vanadium–sulfur.

during the first cycles will induce an increase in the viscosity of the electrolyte and a decrease in its ionic conductivity.[55] As such, the effective mobility of the polysulfides decreases within the electrolyte, which in turn decreases the rate of side reactions and capacity fade of the Li–S cell after ca. 10 cycles. One can notice that in a few of the cells, the specific capacity follows a non-monotonic trend by first increasing and thereafter decreasing. The first phenomenon is explained by an initial increase of the sulfur/carbon contact area induced by the dissolution and precipitation of the polysulfide Li_xS_y during the successive charges and discharges of the Li–S cells. This is particularly the case when the initial sulfur powder is micron-sized, i.e., has a limited surface area, while the conductive additive is has a high surface area (SuperC65 from Imerys G&C = 62 m^2/g). Detailed investigations on this phenomenon will be published in the near future.

The specific capacity of the raw sulfur was reduced to ~267 mAh/g after 100 cycles and the capacity fading was calculated to be 35% from the 30th cycle to the 100th cycle. This is considered to be typical cycling behavior for Li–S cells with liquid electrolytes.[14,39] On the contrary, the capacity fading of the coated sulfur materials was significantly mitigated even after 100 cycles. The specific capacities were recorded at 431 and 365 mAh/g, corresponding to 20% and 24% capacity fading (vs. the 30th cycle) for Alu–S- and Van–S-coated sulfur samples, respectively. The specific capacity fading is undoubtedly and distinctly mitigated for all Li–S cells containing coated sulfur samples, but with a significant difference between the Alu–S and Van–S materials. These results show that the electrochemical performance of the Li–S cells based on the different sulfur samples can be ranked as Alu-S > Van-S > raw sulfur. These results are in agreement with the sample characterization, that is, XPS and NMR.

The mitigation of the capacity fading of Alu–S is significantly higher than that of Van–S (Figure 7D and Table 2). The metal oxide with vanadium could not be
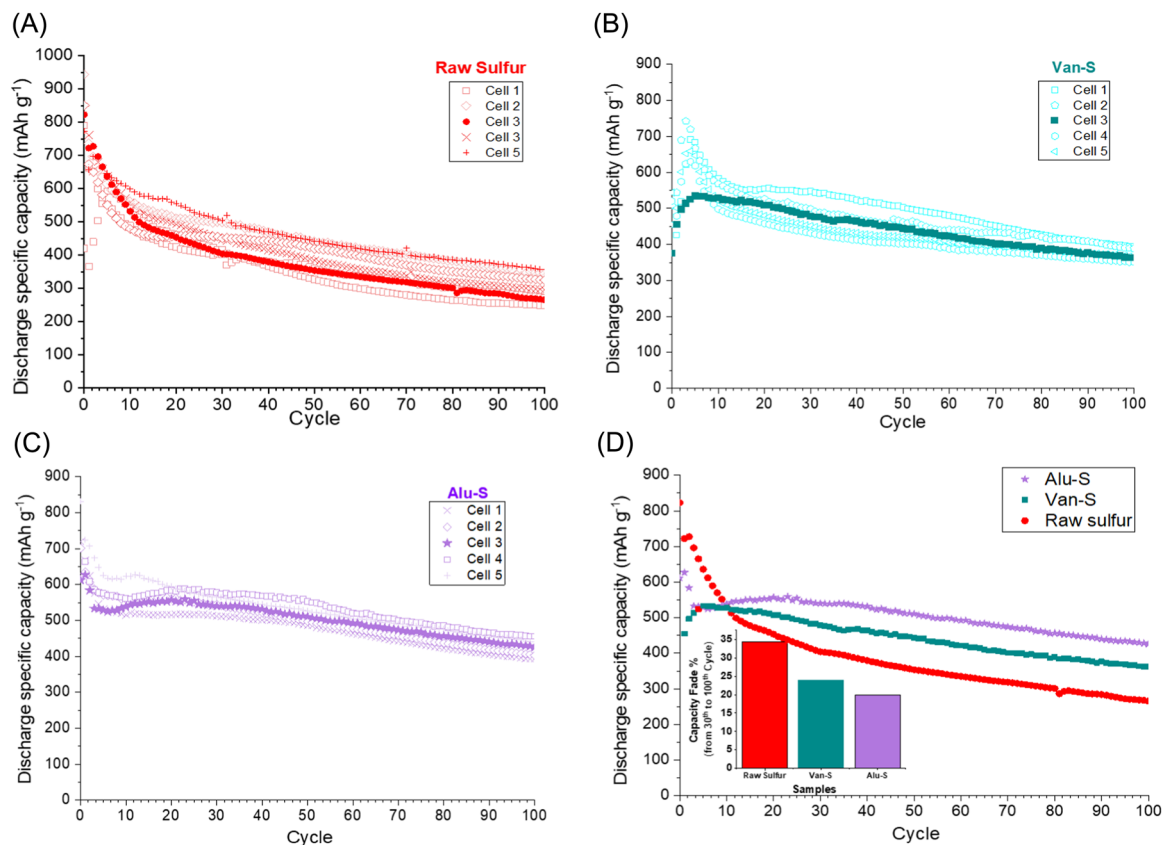
FIGURE 7 Specific discharge capacity at a constant (dis)charge rate (C/10) of Li–S electrodes with different sulfur powders present in the electrode: (A) raw sulfur, (B) Van–S, (C) Alu–S, and (D) comparison between the cycling (C/10). Alu–S, aluminum–sulfur; Van–S, vanadium–sulfur.

TABLE 2 Summary of discharge capacity at 30th and 100th, specific capacity fade, and average Coulombic efficiency between the 30th and 100th cycle for the raw sulfur-, Van–S-, and Alu–S-coated Li–S cells (from Figure 7D and Supporting Information: Figure S5).

Composition	30th Specific discharge capacity (mAh/g)	100th Specific discharge capacity (mAh/g)	Capacity Fade % (from 30th to 100th Cycle)	Capacity Fade per cycle from 30th to 100th Cycle(mAh/g/cycle)	Average coulombic efficiency (from 30th to 100th Cycle)
Raw Sulfur	413	267	35	2.10	98.90
Van-S	480	365	24	1.64	99.10
Alu-S	537	431	20	1.51	99.40

detected (see Figure 5 and related discussion) even if the presence of a coating containing the vanadium element is confirmed (see Figure 4, Supporting Information: Figures S2, S4, and Table 1 and related discussion). In addition, vanadium-based metal oxides are described to be among the most effective metal oxides as polysulfide trappers. However, the effectiveness of partially reacted molecular vanadium (based on our results) appears to be relatively limited. Even the presence of V^{5+} may be detrimental in the long term during battery cycling.[23,47] The gradual consumption of active polysulfides

(Li_xS_y) during the successive charge steps can lead to the formation of electrochemically inert sulfate species by the highly oxidized vanadium species (V^{5+}).[23,47,48] This phenomenon can reasonably explain the higher hysteresis (Figure 8 and Supporting Information: Figure S6) and capacity decay of Van–S cells (Figure 7) in comparison with Alu–S cells. The ^{27}Al-NMR data undoubtedly prove the presence of amorphous alumina (Al_2O_3) in the coating of the Alu–S sample. Based on the literature,[26,41,45] the alumina promotes the adsorption of the solubilized polysulfide on the surface and mitigates
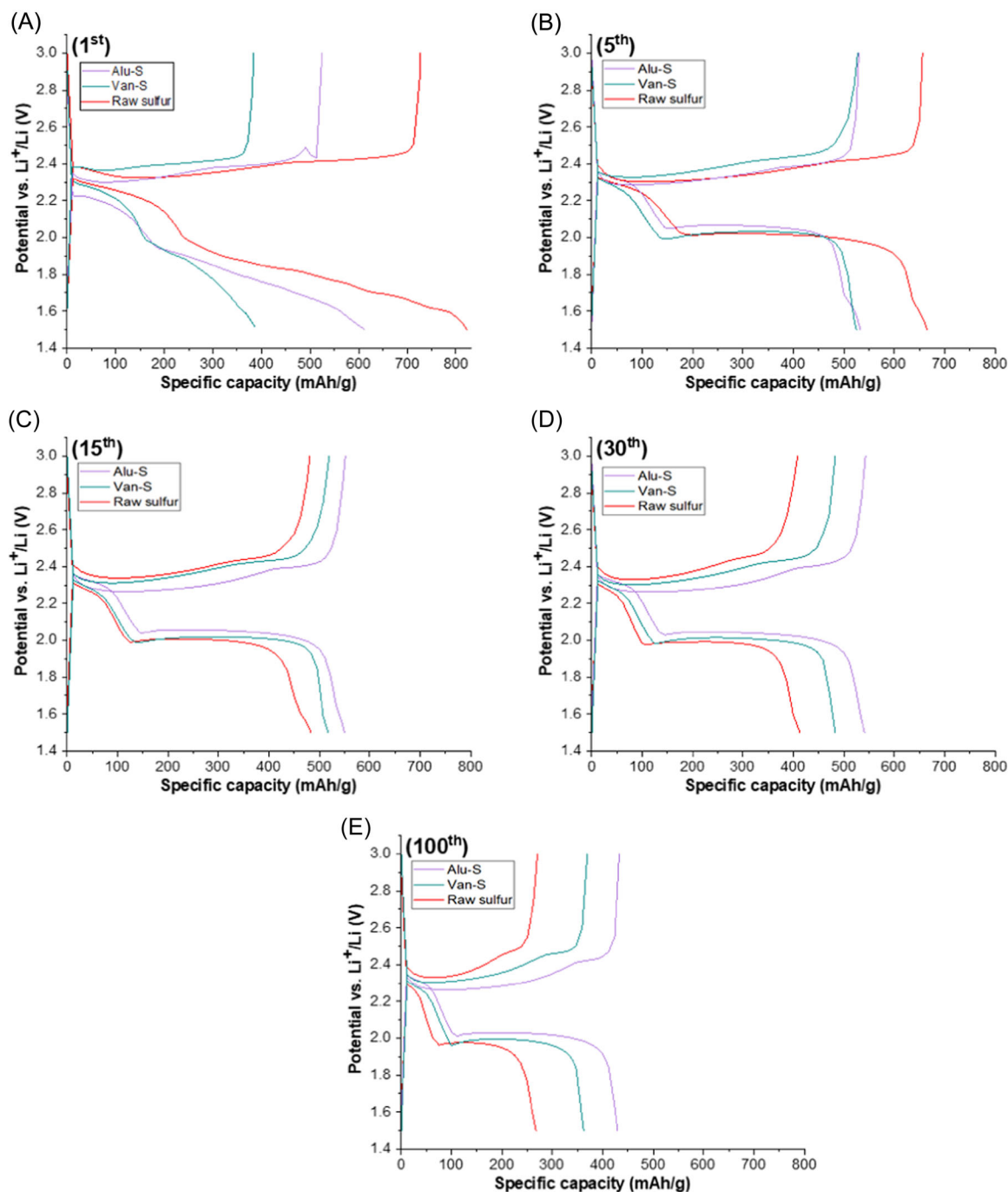
FIGURE 8 Galvanostatic (dis)charge (C/10) profiles of Li–S cells with (Alu–S and Van–S) coated and raw sulfur, respectively, at (A) the 1st, (B) 5th, (C) 15th, (D) 30th, and (E) 100th cycle. Alu–S, aluminum–sulfur; Van–S, vanadium–sulfur.

the polysulfide shuttle phenomenon. Consequently, the capacity fading is mitigated and the performance of Li–S cells containing this Alu–S material is enhanced (Figure 7 and Table 2), even after prolonged (dis)charge cycling, in comparison to the cells using the other sulfur materials. In addition, it has been reported[41,56] that after consecutive charges and discharges, an artificial ion-conductive SEI layer (containing lithium aluminate "$LiAlO_2$" groups) is formed with the alumina-based metal oxide coating. The formation of $LiAlO_2$ not only promotes the high ionic conductivity of cells but also acts as a good polysulfide reservoir, resulting in high utilization and reversibility of sulfur-positive electrodes. Therefore, we consider Alu–S-coated sulfur to be superior to Van–S-coated sulfur as an active material in the sulfur electrode for Li–S cells, taking into account all the electrochemical data (see discussion in Figures 7–10 and Supporting Information: Figure S5–S7).
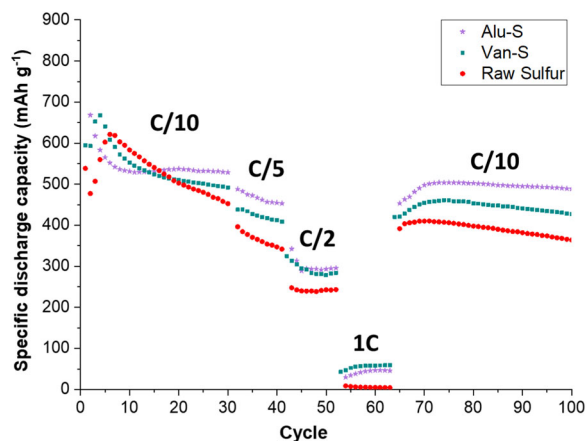
FIGURE 9 Discharge capacity at different discharge/charge rates for Li–S cells using (Alu–S and Van–S) coated and raw sulfur, respectively, in the positive electrode. Alu–S, aluminum–sulfur; Van–S, vanadium–sulfur.
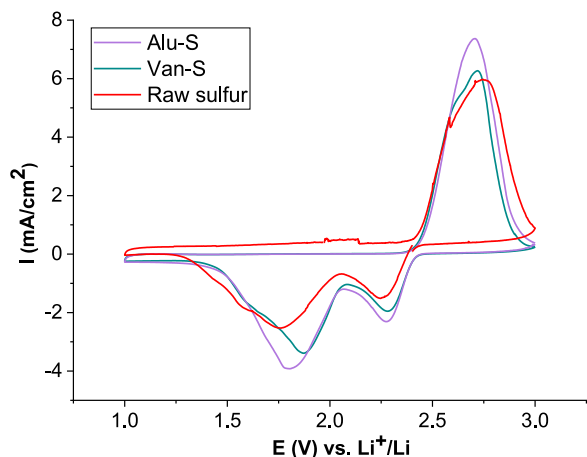

FIGURE 10 Cyclic voltammetry of (Alu–S and Van–S) coated and raw sulfur-based electrodes at 0.1 mV/s. Alu–S, aluminum–sulfur; Van–S, vanadium–sulfur.

Note that in comparison to raw sulfur, the Coulombic efficiency (Supporting Information: Figure S5 and Table 2) through cycling is high (>~99%) and is much more constant with the smallest variation in the case of (Alu–S and Van–S) coated Li–S cells. This also confirms the efficacy of the different coatings by the DBD-plasma process on sulfur powder and the superiority of the Alu–S-coated sulfur sample over the Van–S-coated sulfur sample as an active material in sulfur electrodes. Considering the high sulfur loading (~4.5 mg/cm^2) of our electrodes, the influence of the metal oxide-based coating on sulfur is evident in the performance of the Li–S cells in terms of specific capacity, repeatability, and mitigation of capacity fading, which is in agreement with the literature and the characterization data (Section 3.1).

The initial galvanostatic discharge cycles with (Alu–S and Van–S) and raw sulfur Li–S cells show an irregular profile (Figure 8A), featuring the absence of a potential plateau at 2.0 V versus Li$^+$/Li and the limited discharge capacity showing a continuous potential decrease throughout the discharge process. This phenomenon can be related to the important charge-transfer resistance observed for the EIS analysis (see later Section 3.4). Besides, at the early stage (Figure 8A,B), when compared to the cell with raw sulfur, all cells containing (Alu–S and Van–S) coated sulfur materials present a pronounced overpotential fit with the following trend: $\Delta V_{Alu-S} > \Delta V_{Van-S} > \Delta V_{Raw-sulfur}$. Hence, we believe that the irregular initial galvanotactic profiles of the Li–S cells containing the different coated sulfur materials are due to coating activation or supplementary rearrangement mechanisms induced by the presence of the coatings. As mentioned previously, the formation of an artificial ionic conductive SEI layer containing lithium aluminate "LiAlO$_2$" groups was observed in the literature[41,56] for the electrode containing the Alu–S material. We reported similar aberrant first discharge phenomena in our previous work.[39]

After the 5th cycle (Figure 8B), all coated and raw Li–S cells show typical (dis)charge galvanostatic profiles and the expected trends for charge and discharge of a sulfur electrode in the electrolyte.[39] As reported in the literature,[39,57] two discharge voltage plateaus appear at around 2.3 and 2.1 V versus Li$^+$/Li, which can be assigned to two-step reactions during the discharge process. The overpotential of the Alu–S material disappeared, while it was still significant for Van–S. This can be summarized as $\Delta V_{Van-S} > \Delta V_{Alu-S} \approx \Delta V_{Raw-sulfur}$. Overall, we can consider that at this stage, the specific capacity of the raw sulfur is still superior to that of the coated materials (Figure 7).

After 15 cycles (Figure 8C), all cells show quite similar specific capacity values, between ~500 and 550 mAh/g. The ΔV_{Van-S} is now less significant than during the early cycles. More importantly, Alu–S shows the smallest potential hysteresis (Supporting Information: Figure S6) at this stage, leading to the following order: $\Delta V_{Van-S} > \Delta V_{Raw-sulfur} > \Delta V_{Alu-S}$. All materials, raw and coated sulfur, deliver a similar specific capacity overall.

For the 30th cycle, (on medium-term cycling, Figure 8D), the Li–S cells using Alu–S and Van–S show higher capacities than that of the cells containing the raw sulfur (Table 3). The lower discharge plateau (labeled C$_L$) at ca. 2.0 V versus Li$^+$/Li and the upper discharge plateau (labeled C$_U$) between 2.0 and 2.4 V versus Li$^+$/Li are almost similar for the three samples. We then consider that the presence of the Alu–S and Van–S coatings does not change the electrochemical reactions but acts as an effective barrier to mitigate the capacity fading by hindering the polysulfide shuttle phenomenon. Even

TABLE 3 From Figure 8, values of the upper plateau discharge between 2.0–2.4 V vs. Li$^+$/Li, labeled C_U, the lower discharge plateau at ca. 2.0 V vs. Li$^+$/Li, labeled C_L.

| Composition | 30th Cycle | | | | | 100th Cycle | | | | |
| | (mAh/g) | | | (%) | | (mAh/g) | | | (%) | |
	C_U	C_L	C_T	C_U/C_T	C_L/C_T	C_U	C_L	C_T	C_U/C_T	C_L/C_T
Raw sulfur	99	314	413	24	76	69	198	267	26	74
Van–S	129	351	480	27	73	99	266	365	27	73
Alu–S	142	395	537	26	74	113	318	431	26	74

Note: The total discharge-specific charge is labeled as $C_U + C_L = C_T$ for the 30th and 100th cycles.

after 100 cycles, the shape of the (dis)charge profile of the Li–S cell with Alu–S- and Van–S-coated sulfur samples remains (mostly) constant in contrast to the cells with raw sulfur. At the 100th cycle (Figure 8E), the capacity fade is less evident for the Li–S cells using Alu–S- and Van–S-coated samples compared to the cells made with raw sulfur. A precise analysis of the capacity data between the 30th and 100th cycle (Table 3) shows that the C_U in discharge decreases by 30%, 23%, and 20% for the cells with raw sulfur-, Van–S-, and Alu–S-coated samples (when compared), respectively. Besides, the capacity fade for the C_L part of the discharge is 37%, 24%, and 19%, respectively. Generally, during aging, the cathodic capacity fade is equally represented in C_T and C_L parts of the reduction occurring in the positive electrodes. In addition, the potential hysteresis (Supporting Information: Figure S6) for Li–S cells made of (Alu–S and Van–S) coated and raw sulfur-based positive electrodes increases for all cells during aging. However, the increase in hysteresis is mitigated in the case of the Alu–S-coated sulfur sample at ~15 mV, while it is superior at 25 and 85 mV for Van–S-coated and raw sulfur samples, respectively, confirming the superiority of the Alu–S material.

In summary, Alu–S shows larger discharge capacity and lower capacity fading, indicating the effectiveness of a metal oxide-based coating that is more profitable for utilization as the active material. Moreover, the potential gap (hysteresis) between the discharge and charge plateaus is narrow and relatively stable, suggesting that the system has smaller polarization and higher reaction kinetics. This is because sulfur is effectively confined by the metal oxide-based coating, which provides protection by restricting the diffusion of intermediate polysulfides to the electrolyte, and these results are in agreement with the literature.[26,41,44,45]

Figure 9 and Supporting Information: Figure S7 compare the evolution of the discharge capacity versus current density between the Li–S cells with (Alu–S and Van–S) coated and raw sulfur present in the positive electrode. As anticipated, increasing the current density lowers the capacity. Besides, in comparison with raw sulfur, the rate capability of the Li–S cells using the coated sulfur powders (Supporting Information: Figure S7F) is higher. In Figure 9, to determine the influence of different coatings, one cycle at each C-rate (i.e., C/2, C/5, C/10) has been compared for (Alu–S and Van–S) coated and raw sulfur-based cells. The rate capability of the Li–S cells can be classified as follows: Alu–S > Van–S > Raw sulfur-based Li–S cells. The cells using raw sulfur (at C/10 and C/5) show an overall pronounced increase of the hysteresis between charge and discharge in comparison to cells using coated Alu–S and Van–S materials (Supporting Information: Figure S7A–E). As mentioned in our previous publications,[14,39] on reaching the 1C rate, all coated and uncoated sulfur cells show insignificant capacity values. This might be explained by the (relatively bigger) particle size of the sulfur powders and the high sulfur loading of ~4.5 mg/cm^2 in Li–S electrodes, which potentially hinders the reduction and/or oxidation process involving sulfur in the positive electrode. Note that capacity is retained for all cells when switched back to the C/10 rate.

To evaluate the effect of the different metal oxide-based coated sulfur samples on the kinetics of the electrochemical reactions occurring in the Li–S cells during the cycling, cyclic voltammetry (CV) at a 0.1 mV/s scan rate was measured (Figure 10). As expected, the shapes of the CV using electrodes containing either Alu–S- and Van–S-coated or raw sulfur are overall similar, with one anodic peak at ca. 2.50 V versus Li$^+$/Li and two reduction peaks at ca. 2.25 and 1.85 V versus Li$^+$/Li.[14,45,58] For all coated and raw sulfur samples, two reduction peaks at 2.25 V versus Li$^+$/Li and 1.85 V versus Li$^+$/Li appear during the first cathodic scan, which is assigned to the reduction of sulfur to higher-order (soluble) lithium polysulfides (Li_2S_6 and Li_2S_8) and further reduction to lower-order (insoluble) lithium polysulfides (Li_2S and Li_2S_2), respectively. During the

anodic scan, only one sharp oxidation peak at 2.50 V versus Li^+/Li is observed, which corresponds to the conversion of Li_2S_2 and Li_2S into Li_2S_8 and sulfur.

The peak intensities of the CV (Figure 10) are clearly influenced by the presence of a coating on the sulfur particles. In comparison to the raw sulfur electrode, Alu–S- and Van–S-coated sulfur electrodes show distinct sharp peaks with a clear positive shift in the reduction peak, which indicates that the coating, even though not conductive, can cause a decrease in cell polarization and enhanced kinetics for the reaction of sulfur with lithium. This is attributed to closer contact between the sulfur species (solid and liquid) and the coating (physical membrane and chemical polysulfide trapper) than between the sulfur species and the conductive carbon additive. Compared to coated sulfur, the oxidation peak of raw sulfur shows a more positive peak value because of the greater formation of insoluble Li_2S, which can block pores and causes polarization during the Li-ion diffusion. This phenomenon strongly suggests that thin coatings mitigate the "shuttle effect," with the ion conductivity of coated electrodes preserved.[41] In addition, the higher peak current and sharper peak profile of the Alu–S-coated sample reveal more pronounced and homogeneous electrochemical reactivity, respectively. This can be attributed to better wetting of the electrode due to favorable interactions between the electrolyte, both the polar organics (DOL and DME) and Li-TFSI (dissolved salt), and the alumina present in the coating and the formation of a $Li–Al_xO_y$ alloy (Li-ion conductive) in the coating, thus facilitating Li-ion transport.[26,41,56] Consequently, it seems to be clear that the kinetics of the electrochemical reactions of the sulfur species in the Li–S cells can be classified as Alu-S > Van-S > Raw sulfur. Besides, no additional reduction or oxidation peaks were observed in Figure 10, which shows that the metal oxide-based coatings are not electroactive between 1.0 and 3.0 V and serve as an adsorbent.[26,41] In addition, anodic linear sweep voltammetry (LSV) from 1.5 to 5.0 V versus Li^+/Li with bare Al foils and coated Al foils with activated (aluminum and vanadium) alkoxide films (Supporting Information: Figure S8) showed similar results without inducing any additional reaction and are stable in the potential range used to test Li–S cells, with the anodic reaction starting (as expected) at a voltage above 4.5 V versus Li^+/Li, attributed to the degradation of the electrolyte at this potential.

3.4 | Electrochemical impedance spectroscopy (EIS)

In Figure 11, the results of the EIS test are presented for Li–S cells made of raw or Alu–S- and Van–S-coated sulfur electrodes before the first (dis)charge and after 30 galvanostatic cycles. The EIS spectra of pristine electrodes (Figure 11A) show one semicircle in the high-frequency region, which is attributed to the electrode–electrolyte interface of the sulfur electrode in the absence of any significant faradic process. The cells with Alu–S and Van–S electrodes show resistance values at ~25 and 32 Ω, respectively, which are significantly smaller than the electrode containing the raw sulfur ~52 Ω. Similarly, for the metal oxide-based Alu–S-coated sulfur, the slope of the following inclined lines (known as the Warburg element) is significantly steeper than that of the raw sulfur and Van–S samples. It appears that both the electron transfer and the Li-ion transport in the sulfur electrodes are promoted in the presence of Alu–S-coated sulfur. This is in agreement
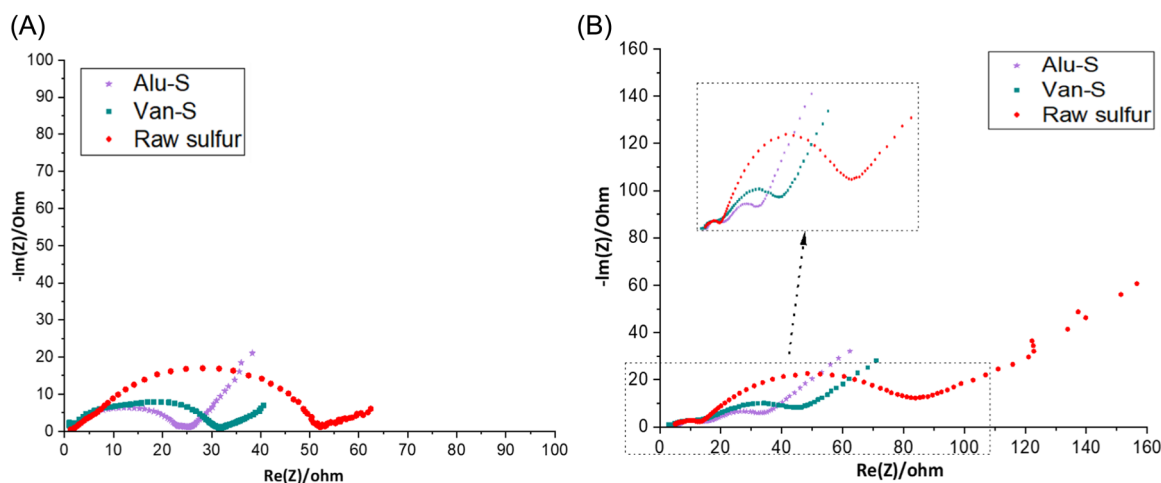

FIGURE 11 Nyquist plots for Li–S cells at OCV using (Alu–S and Van–S) coated and raw sulfur-based (A) pristine electrodes and (B) the same electrodes after 30 galvanostatic cycles at C/10. Alu–S, aluminum–sulfur; Van–S, vanadium–sulfur.

with the literature[26,44,59] and the discussion presented in Sections 3.1 and 3.3.

In Figure 11B, the shape of the Nyquist plots of electrodes after 30 cycles (discharge) evolved radically due to major changes in the electrodes with the successive dissolution–precipitation mechanisms of the sulfur species. After the 30th cycle, the impedance spectrum has two depressed semicircles and an inclined line. The contact (interfacial) resistances (R_c) in the sulfur porous electrode can be associated with the first semicircle at a higher frequency. All sulfur-coated electrodes show decreased R_c values (the first semicircle at higher frequencies; the diameter shrinks), with Alu–S showing the lowest R_c value, in comparison to the raw sulfur electrodes. The second semicircle in the middle-frequency range might be attributed to an effective charge-transfer resistance (R_{ct}) for the long- and short-chain polysulfides. It is again significantly smaller for the metal oxide-based coated sulfur materials than the raw sulfur material and it can be classified as $R_{ct\,(Alu-S)} < R_{ct\,(Van-S)} < R_{ct\,(Raw\,sulfur)}$. Besides, we observe that both coated and uncoated aged Li–S cells show increased electrolyte resistance (limited to several ohms), possibly due to the change in the bulk transport properties induced by the change in the electrolyte composition in the presence of polysulfides. The EIS results are in good agreement with what we observed in the material and electrochemical characterizations (Sections 3.1 and 3.3) of these cells.

4 | CONCLUSIONS

In this work, we have successfully performed surface modification of raw sulfur particles. We demonstrated the concept of coating by activation of metal alkoxides by using DBD-plasma technology. The dry process involves the solvent-free batch production of coated sulfur powder under ambient pressure and low-temperature conditions. The DBD-plasma dry coating is close to kilogram scale, sustainable, and compatible with upscaling. Two different (Alu–S and Van–S) coatings were produced and characterized and their impact on the properties of sulfur powders was investigated. SEM and EDX characterizations confirmed the presence and the homogeneous distribution of the coating and the metal element on the surface of the sulfur particles. The coatings are very thin, have thicknesses of several nanometers, and are composed of the different elements present in the metal alkoxide precursor, that is, the metal (Al or V), oxygen, and nonconductive sp^3 carbon as confirmed by EDX analysis. The top surface of the sulfur particles appears to be oxidized, but no significant detrimental effect was observed on the battery performance. Solid-state NMR experiments proved the

presence of alumina Al_2O_3 metal oxide, but no vanadium oxide could be detected. Among these, the Alu–S metal oxide-based coated sulfur powder shows the best electrochemical performance in Li–S cells. Besides, the surface modification process did not influence the bulk crystalline properties and morphology of the core particles.

Our results show that the electrochemical performance of the Li–S cells could be improved by metal oxide coating (with high sulfur loading ~4.5 mg/cm^2) in terms of capacity fading and reproducibility. The kinetics of the electrochemical reactions during the cycling of the Li–S cells can be ranked as Alu-S > Van-S > Raw sulfur. This marks Alu–S as the superior metal oxide-based coating in terms of higher capacity fading mitigation and kinetics of sulfide-species oxidation/reduction (i.e., rate capability, CV tests). These results are supported by EIS investigations that confirmed that the surface modification with Alu–S provided the lowest contact (interfacial) and charge-transfer resistance in the corresponding sulfur electrode as well as efficient Li-ion transport in the electrolytic solution. More importantly, the environmentally friendly electrode preparation process (i.e., use of an aqueous binder), combined with the advantage of using DBD plasma technology, could be compatible with and cost-effective for pouch cell production. We conclude that our straightforward surface functionalization process using DBD plasma technology is suitable for different types of coatings on sulfur particles under dry and low-temperature conditions, which makes it suitable to fulfill the urgent need for development of more sustainable technologies.

AUTHOR CONTRIBUTIONS

Ahmed Shafique: Investigation; visualization; validation; writing & editing—original draft. **Annick Vanhulsel**: Review & editing; validation. **Vijay Shankar Rangasamy**: Review & editing, validation. **Mohammadhosein Safari**: Review & editing; validation. **Kitty Baert**: XPS analysis; review & editing; validation. **Tom Hauffman**: XPS analysis; review & editing; validation. **Peter Adriaensens**: NMR analysis; review & editing; validation. **Marlies K. Van Bael**: Review & editing; validation. **An Hardy**: Supervision; review & editing; validation. **Sébastien Sallard**: Conceptualization; supervision; review & editing; validation.

CONFLICT OF INTEREST STATEMENT
The authors declare no conflict of interest.

DATA AVAILABILITY STATEMENT
Research data are not shared.

ORCID
Sébastien Sallard http://orcid.org/0000-0001-8025-8519

REFERENCES

1. Stampatori D, Raimondi PP, Noussan M. Li-ion batteries: a review of a key technology for transport decarbonization. *Energies.* 2020;13:2638.

2. Larcher D, Tarascon JM. Towards greener and more sustainable batteries for electrical energy storage. *Nat Chem.* 2014;7:19-29.

3. Placke T, Kloepsch R, Dühnen S, Winter M. Lithium ion, lithium metal, and alternative rechargeable battery technologies: the odyssey for high energy density. *J Solid State Electrochem.* 2017;21:1939-1964.

4. Kang W, Deng N, Ju J, et al. A review of recent developments in rechargeable lithium-sulfur batteries. *Nanoscale.* 2016;8: 16541-16588.

5. Balach J, Linnemann J, Jaumann T, Giebeler L. Metal-based nanostructured materials for advanced lithium–sulfur batteries. *J Mater Chem A.* 2018;6:23127-23168.

6. Rosenman A, Markevich E, Salitra G, Aurbach D, Garsuch A, Chesneau FF. Review on Li-Sulfur battery systems: an integral perspective. *Adv Energy Mater.* 2015;5:1500212.

7. Li T, Bai X, Gulzar U, et al. A comprehensive understanding of lithium–sulfur battery technology. *Adv Funct Mater.* 2019;29:1901730.

8. Tarascon J-M, Armand M. Issues and challenges facing rechargeable lithium batteries. *Nature.* 2001;414:359.

9. Yin YX, Xin S, Guo YG, Wan LJ. Lithium-sulfur batteries: electrochemistry, materials, and prospects. *Angew Chem Int Ed.* 2013;52:13186-13200.

10. Zhu K, Wang C, Chi Z, et al. How far away are lithium-sulfur batteries from commercialization? *Front Energy Res.* 2019;7:123.

11. Xiang Y, Li J, Lei J, et al. Advanced separators for lithium-ion and lithium-sulfur batteries: a review of recent progress. *ChemSusChem.* 2016;9:3023-3039.

12. Peng HJ, Huang JQ, Cheng XB, Zhang Q. Review on high-loading and high-energy lithium–sulfur batteries. *Adv Energy Mater.* 2017;7:1700260.

13. Chung SH, Chang CH, Manthiram A. Progress on the critical parameters for lithium–sulfur batteries to be practically viable. *Adv Funct Mater.* 2018;28:1801188.

14. Shafique A, Rangasamy VS, Vanhulsel A, et al. The impact of polymeric binder on the morphology and performances of sulfur electrodes in lithium–sulfur batteries. *Electrochim Acta.* 2020;360:136993.

15. Li Y, Shapter JG, Cheng H, Xu G, Gao G. Recent progress in sulfur cathodes for application to lithium–sulfur batteries. *Particuology.* 2021;58:1-15.

16. Liu T, Hu H, Ding X, et al. 12 years roadmap of the sulfur cathode for lithium sulfur batteries (2009-2020). *Energy Storage Mater.* 2020;30:346-366.

17. Chen J, Zhang Q, Shi Y, et al. A hierarchical architecture S/MWCNT nanomicrosphere with large pores for lithium sulfur batteries. *Phys Chem Chem Phys.* 2012;14:5376-5382.

18. Mohanty SP, Kishore B, Nookala M. Composites of sulfur-titania nanotubes prepared by a facile solution infiltration route as cathode material in lithium-sulfur battery. *J Nanosci Nanotechnol.* 2018;18:6830-6837.

19. Guo J, Xu Y, Wang C. Sulfur-impregnated disordered carbon nanotubes cathode for lithium–sulfur batteries. *Nano Lett.* 2011;11:4288-4294.

20. Zhang C, Liu D-H, Lv W, et al. A high-density graphene–sulfur assembly: a promising cathode for compact Li-S batteries. *Nanoscale.* 2015;7:5592-5597.

21. Xue M, Zhou Y, Geng J, et al. Hollow porous SiO_2 nanobelts containing sulfur for long-life lithium-sulfur batteries. *RSC Adv.* 2016;6:91179-91184.

22. Wu DS, Shi F, Zhou G, et al. Quantitative investigation of polysulfide adsorption capability of candidate materials for Li-S batteries. *Energy Storage Mater.* 2018;13:241-246.

23. Tadayon N, Ramazani A, Torabi M, Seyyedin ST. Using of various metal species for improvement of electrochemical performances of lithium sulfur batteries. *J Electroanal Chem.* 2020;878:114652.

24. Zhang Y, Bakenov Z, Zhao Y, et al. One-step synthesis of branched sulfur/polypyrrole nanocomposite cathode for lithium rechargeable batteries. *J Power Sources.* 2012;208:1-8.

25. Choi YJ, Jung BS, Lee DJ, et al. Electrochemical properties of sulfur electrode containing nano Al_2O_3 for lithium/sulfur cell. *Phys Scr.* 2007;T129:62-65.

26. Dong K, Wang S, Zhang H, Wu J. Preparation and electrochemical performance of sulfur-alumina cathode material for lithium-sulfur batteries. *Mater Res Bull.* 2013;48: 2079-2083.

27. Fan X, Sun W, Meng F, Xing A, Liu J. Advanced chemical strategies for lithium–sulfur batteries: a review. *Green Energy Environ.* 2018;3:2-19.

28. Liu X, Huang JQ, Zhang Q, Mai L. Nanostructured metal oxides and sulfides for lithium–sulfur batteries. *Adv Mater.* 2017;29:1601759.

29. Qu Q, Gao T, Zheng H, et al. Strong surface-bound sulfur in conductive MoO_2 matrix for enhancing Li-S battery performance. *Adv Mater Interfaces.* 2015;2:1500048.

30. Tao X, Wang J, Liu C, et al. Balancing surface adsorption and diffusion of lithium-polysulfides on nonconductive oxides for lithium–sulfur battery design. *Nat Commun.* 2016;7:11203.

31. Chen Y, Wang T, Tian H, Su D, Zhang Q, Wang G. Advances in lithium–sulfur batteries: from academic research to commercial viability. *Adv Mater.* 2021;33:2003666.

32. Deng H, Yao L, Huang QA, et al. Facile assembly of a S@carbon nanotubes/polyaniline/graphene composite for lithium–sulfur batteries. *RSC Adv.* 2017;7:9819-9825.

33. Wang J, Wang W, Li H, Tan T, Wang X, Zhao Y. Carbon nanotubes/SiC prepared by catalytic chemical vapor deposition as scaffold for improved lithium-sulfur batteries. *J Nanopart Res.* 2019;21:113.

34. Gu X, Lai C. Recent development of metal compound applications in lithium-sulphur batteries. *J Mater Res.* 2018;33:16-31.

35. Yan B, Li X, Bai Z, et al. A review of atomic layer deposition providing high performance lithium sulfur batteries. *J Power Sources.* 2017;338:34-48.

36. Kim H, Lee JT, Lee D-C, Magasinski A, Cho W, Yushin G. Plasma-enhanced atomic layer deposition of ultrathin oxide coatings for stabilized lithium-sulfur batteries. *Adv Energy Mater.* 2013;3:1308-1315.

37. Dörfler S, Althues H, Härtel P, Abendroth T, Schumm B, Kaskel S. Challenges and key parameters of lithium-sulfur batteries on pouch cell level. *Joule.* 2020;4:539-554.

38. Hu Y, Chen W, Lei T, et al. Strategies toward high-loading lithium–sulfur battery. *Adv Energy Mater.* 2020;10:2000082.

39. Shafique A, Rangasamy VS, Vanhulsel A, et al. Dielectric barrier discharge (DBD) plasma coating of sulfur for mitigation of capacity fade in lithium–sulfur batteries. *ACS Appl Mater Interfaces.* 2021;13:28072-28089.

40. Shafique A, Vanhulsel A, Rangasamy VS, et al. Impact of different conductive polymers on the performance of the sulfur positive electrode in Li–S batteries. *ACS Appl Energy Mater.* 2022;5:4861-4876.

41. Li X, Liu J, Wang B, et al. Nanoscale stabilization of Li-sulfur batteries by atomic layer deposited Al_2O_3. *RSC Adv.* 2014;4:27126-27129.

42. Han X, Xu Y, Chen X, et al. Reactivation of dissolved polysulfides in Li-S batteries based on atomic layer deposition of Al_2O_3 in nanoporous carbon cloth. *Nano Energy.* 2013;2:1197-1206.

43. Zhu M, Li S, Liu J, Li B. Promoting polysulfide conversion by V_2O_3 hollow sphere for enhanced lithium-sulfur battery. *Appl Surf Sci.* 2019;473:1002-1008.

44. Xu J, Jin B, Li H, Jiang Q. Sulfur/alumina/polypyrrole ternary hybrid material as cathode for lithium-sulfur batteries. *Int J Hydrogen Energy.* 2017;42:20749-20758.

45. Yu M, Yuan W, Li C, Hong JD, Shi G. Performance enhancement of a graphene–sulfur composite as a lithium–sulfur battery electrode by coating with an ultrathin Al_2O_3 film via atomic layer deposition. *J Mater Chem A.* 2014;2:7360-7366.

46. Sun F, Qu Z, Wang H, et al. Vapor deposition of aluminium oxide into N-rich mesoporous carbon framework as a reversible sulfur host for lithium-sulfur battery cathode. *Nano Res.* 202014:131-138.

47. Liu M, Li Q, Qin X, et al. Suppressing self-discharge and shuttle effect of lithium–sulfur batteries with V_2O_5-decorated carbon nanofiber interlayer. *Small.* 2017;13:1602539.

48. Liang X, Kwok CY, Lodi-Marzano F, et al. Tuning transition metal oxide-sulfur interactions for long life lithium sulfur batteries: the "Goldilocks" principle. *Adv Energy Mater.* 2016;6:1501636.

49. Kundu S, Satpati B, Mukherjee M, Kar T, Pradhan SK. Hydrothermal synthesis of polyaniline intercalated vanadium oxide xerogel hybrid nanocomposites: effective control of morphology and structural characterization. *New J Chem.* 2017;41:3634-3645.

50. O'Dell LA, Savin SLP, Chadwick AV, Smith ME. A 27Al MAS NMR study of a sol–gel produced alumina: identification of the NMR parameters of the θ-Al_2O_3 transition alumina phase. *Solid State Nucl Magn Reson.* 2007;31:169-173.

51. Kříž O, Čásenský B, Lyčka A, Fusek J, Heřmánek S. 27 Al NMR behavior of aluminium alkoxides. *J Magn Reson.* 1984;60:375-381.

52. Dubey RK, Meenakshi, Singh AP. Synthesis, spectroscopic [IR, (1H, 13C, 27Al) NMR] and mass spectrometric studies of aluminium(III) complexes containing O- and N-chelating Schiff bases. *Main Group Metal Chemistry.* 2015;38:17-25.

53. Ferreira AR, Küçükbenli E, Leitão AA, De Gironcoli S. Ab initio 27Al NMR chemical shifts and quadrupolar parameters for Al_2O_3 phases and their precursors. *Phys Rev B: Condens Matter Mater Phys.* 2011;84:235119.

54. Pecharromán C, Sobrados I, Iglesias JE, González-Carreño T, Sanz J. Thermal evolution of transitional aluminas followed by NMR and IR spectroscopies. *J Phys Chem B.* 1999;103:6160-6170.

55. Qu C, Chen Y, Yang X, Zhang H, Li X, Zhang H. $LiNO_3$-free electrolyte for Li-S battery: a solvent of choice with low K_{sp} of polysulfide and low dendrite of lithium. *Nano Energy.* 2017;39:262-272.

56. Xiao X, Lu P, Ahn D. Ultrathin multifunctional oxide coatings for lithium ion batteries. *Adv Mater.* 2011;23:3911-3915.

57. Zhu J, Zhu P, Yan C, Dong X, Zhang X. Recent progress in polymer materials for advanced lithium-sulfur batteries. *Prog Polym Sci.* 2019;90:118-163.

58. Wu F, Chen J, Chen R, et al. Sulfur/polythiophene with a core/shell structure: synthesis and electrochemical properties of the cathode for rechargeable lithium batteries. *J Phys Chem C.* 2011;115:6057-6063.

59. Maletti S, Podetti FS, Oswald S, et al. LiV_3O_8-based functional separator coating as effective polysulfide mediator for lithium-sulfur batteries. *ACS Appl Energy Mater.* 2020;3:2893-2899.

SUPPORTING INFORMATION

Additional supporting information can be found online in the Supporting Information section at the end of this article.